Journal of Applied Electrochemistry **31**: 1109–1116, 2001.

Electrodeposition of Sn and Co coatings from citrate solutions

A. SURVILA*, Z. MOCKUS, R. JUŠKĖNAS and V. JASULAITIENĖ
Institute of Chemistry, A. Goštauto 9, LT 2600 Vilnius, Lithuania
*(*author for correspondence, fax: +3702 617018, e-mail: arvydass@ktl.mii.lt)*

Received 21 November 2000; accepted in revised form 29 May 2001

Key words: cobalt, codeposition, citrate, kinetics, tin

Abstract

Optimal conditions for Sn and Co codeposition were achieved in slightly acid citrate solutions containing no excess of ligand. Sn–Co coatings were deposited with amounts of Co ranging from 15 to 86 mass %. Bright deposits were obtained when the Co content exceeded 76%. These coatings may be considered as solid solutions of tin in α-Co and β-Co. The β-Sn phase is predominant in the case of coatings containing less Co. Voltammograms of the partial processes of Sn(II) and Co(II) reduction may be described quantitatively with the proviso that SnL^{2-} and $CoLH^{-}$ are electrically active complexes.

1. Introduction

Electrolytic deposition of tin and its alloys has found extensive application in modern electroplating. Some outstanding properties of tin such as nontoxicity, high corrosion resistance and a good solderability are characteristic of most tin alloys. At the same time, codeposition of tin with another metal makes it possible to obtain coatings with additional useful properties. One example is Sn–Co alloy, which is noted for its increased hardness, colour and lustre, similar to those of chromium coatings [1–6]. Though the first promising experiments in Sn–Co codeposition were performed in 1951 [7], it was not until 20 years later that a commercially viable bath was produced [8, 9]. It is interesting that the first patents were obtained much earlier [10–12].

A great variety of compositions was tested [1–21]. One group of solutions contained only simple inorganic salts such as sulphates, fluorides, chlorides, fluoborates, pyrophosphates and cyanides which may be treated as weak ligands with the exception of the last two. Although fluoride forms comparatively weak complexes with Sn^{2+}, this effect inhibits the oxidation of Sn(II) to Sn(IV) [13]. Stronger complexes give rise to some undesirable phenomena. The use of cyanides, for example, those that are able to form stable complexes with Co(II), leads to a significant decrease in the Co content of the coatings [1].

Gluconate, glucoheptonate, tartrate, citrate and some amines are organic ligands used in plating baths [1–6, 10–12, 16, 20]. To make coatings brighter, various additives, such as butynediol, sintanol, formaldehyde, have been used [17, 18, 21]. It should be noted that it is possible to obtain bright coatings even in the absence of special brighteners [9, 16].

Attention in the investigations cited was focused on problems of an applied nature, underlining the influence of the solution composition and electrolysis conditions on the phase and elemental composition of coatings. A theoretical analysis of kinetics and the mechanism of electrode processes was often omitted. An attempt to analyse such problems has recently been made [22] on codeposition of Sn and Co from citrate solutions. This work deals with further investigations into the above system and presents data further to [22].

2. Experimental details

Solutions were prepared using triply distilled water, $SnSO_4$, $CoSO_4 \cdot 7H_2O$, $K_3C_6H_5O_7 \cdot H_2O$ and Na_2SO_4 (analytical grade). The latter component (0.3 M) was used as supporting electrolyte. The required pH was obtained by adding H_2SO_4 or NaOH. Investigations were performed at 18 ± 2 °C with freshly prepared deaerated solutions. The Sn(II) concentration was adjusted by iodometric titration.

A standard three-electrode cell was used. A platinum plate (1 cm^2 in area) fused into a glass holder served as the substrate for the working electrode. It was plated with a 2–3 μm thick copper underlayer and then with a 5 μm thick tin layer. A rotating disc electrode was prepared in the same way. A platinum plate of 5 cm^2 served as an auxiliary electrode and the saturated Ag/AgCl, KCl electrode was used as reference. All values of potential are given with respect to SHE.

Voltammetric characteristics were recorded at a potential sweep rate of 2 mV s^{-1} by means of a PI 50-1 potentiostat and a KSP-4 recorder (Russia).

Coatings deposited on copper substrate in solutions containing 0.3 M H_3BO_3, as buffer, were used for both elemental and phase analysis. The former was performed by X-ray photoelectron spectroscopy (spectrometer ESCALAB-MK11, England). The source of excitation was a double anode with AlK_α line radiation whose energy was 1486.6 eV and power 300 W (15 kV, 20 mA). The spectrometer was calibrated against Cu $2p_{3/2}$ at 932.4 ± 0.1 eV, Ag $3d_{5/2}$ at 368.0 ± 0.1 eV and Au $4f_{7/2}$ at 83.6 ± 0.1 eV. The pressure in the UHV analyser chamber was maintained at 1.33×10^{-7} Pa. Spectra for every element were recorded 3–5 times and the data obtained were averaged and compared with standards [23]. The thickness of the layer analysed ranged from 1 to 2 nm. Before recording the spectra, the surfaces of samples (~5 nm) were etched with a 5 keV Ar^+ ion stream. The amount (atomic percentage) of each element was calculated from the integral areas of the photoelectron peaks, their sensitivity factors being taken from the operating instructions of the equipment used.

X-ray diffraction (XRD) patterns were measured with a DRON-2.0 diffractometer using CoK_α radiation selected by a secondary graphite monochromator. A continuous scan mode was used within the range $30° \leqslant 2\theta \leqslant 120°$ and at a scan rate of $1°\ 2\theta\ \text{min}^{-1}$. When broad XRD peaks were obtained (see below), Co–Sn coatings were removed from the substrate, ground and heated at 300 °C. However, this procedure did not make the peaks sharper.

3. Some theoretical aspects

Favourable conditions for codeposition of two metals are usually achieved when their equilibrium potentials (E_{eq}^{Sn} and E_{eq}^{Co} in the case of the system under discussion) are close. The difference between $Sn|Sn^{2+}$ and $Co|Co^{2+}$ standard potentials is 0.14 V. It follows from the Nernst equation that $[Sn^{2+}] \approx 10^{-5}\ [Co^{2+}]$ at $E_{eq}^{Sn} = E_{eq}^{Co}$. From the practical point of view, solutions prepared on the basis of simple salts are far from ideal.

To realize this condition in citrate solutions, the concentration of ligand (citrate) should be properly chosen. As has been shown in [22], the potentials mentioned are close in solutions in which Sn(II) is properly complexed and the most of the Co(II) is in the form of aqua-ions. Such solutions should contain no excess of ligand in a slightly acid medium.

The second factor determining the rate of electroreduction of the two metals is of a kinetic nature and is closely related to the mechanism and kinetic parameters of partial electrode processes. According to [22], two species containing Sn(II), that is, $SnLH^-$ and SnL^{2-}, may be treated as electrically active complexes (EAC) taking part in the charge transfer process. At the same time, $CoLH^-$ was found to take part in the partial process of Co(II) reduction. Here citric acid is denoted by the symbol LH_4 (when dissociating it can release up to four protons). In general, charge transfer processes may be represented as follows:

$$MLH_m^{m-2} + 2\ e^- \rightarrow M + L^{4-} + mH^+ \qquad (1)$$

where M^{2+} is Sn^{2+} or Co^{2+}, m is equal to 0 or 1 for Sn(II) reduction and $m = 1$ for Co(II) reduction. Then the kinetic equation for the process (1) takes the form

$$i = i_0 \left\{ \frac{[MLH_m^{m-2}]_s}{[MLH_m^{m-2}]_b} \exp\left(\frac{\alpha n F}{RT}\eta\right) - \frac{[L^{4-}]_s [H^+]_s^m}{[L^{4-}]_b [H^+]_b^m} \times \exp\left(-\frac{(1-\alpha)nF}{RT}\eta\right) \right\} \qquad (2)$$

where the surface and bulk concentrations of species are indicated by the subscripts s and b, respectively, i_0 is the exchange current density, α is the cathodic charge transfer coefficient, and the number of electrons transferred $n = 2$. The cathodic current density i and cathodic overvoltage η are assumed to be positive.

It follows from Equation 2, at sufficiently high overvoltages, that

$$\log(i/c_s) = \log i_0 - \log c_b + \alpha n F \eta / 2.303\, RT \qquad (3)$$

where c is the concentration of the electrically active complex (EAC) given on the left side of Equation 1. Thus, Tafel plots normalized to the surface concentration of EAC may be constructed by means of experimental voltammograms and model simulations.

Surface concentrations may be obtained on the basis of the theoretical model which describes the mass transport of chemically interacting species. Consideration of Fick's second law supplemented by kinetic terms (for details see [24, 25]) has shown that a linear profile of total metal concentration occurs in the Nernst diffusion layer. At the same time, the total ligand concentration remains constant and equal to that in the bulk solution. The latter statement is also valid for proton donors and acceptors. Material balance equations following from this model makes it possible to obtain surface concentrations of all the components as i functions [22, 24–27].

4. Voltammetric characteristics of the system

According to [22], various species are formed in citrate solutions of Sn(II) and Co(II) including aqua-ions of Sn^{2+} and Co^{2+}, complexes SnL^{2-}, $SnLH^-$, $CoLH^-$, $CoLH_2$ as well as different forms of protonated ligand. Molar fractions of components listed are complicated functions of the total concentration of Sn(II), Co(II), ligand and bulk pH. Moreover, the system composition at the electrode surface may differ radically from that in the bulk, depending on the current density. Such effects are controlled by the regularities of mass transport of chemically interacting particles. They are responsible

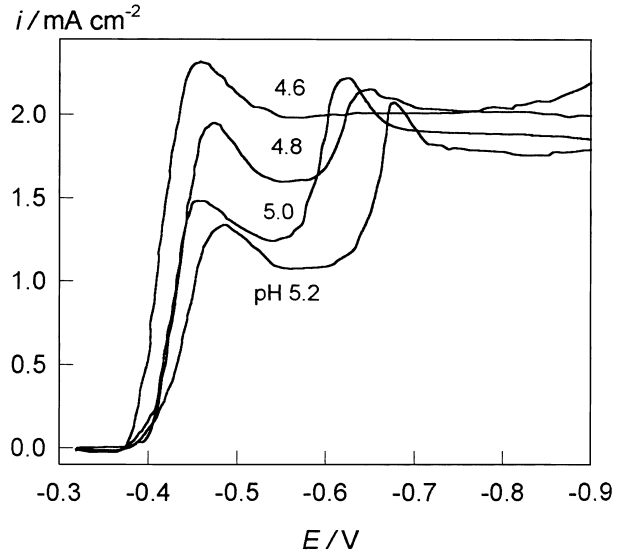

Fig. 1. Experimental voltammograms of Sn(II) reduction recorded under natural convection conditions at various pH. Sn(II) 0.05 M; Cit 0.07 M.

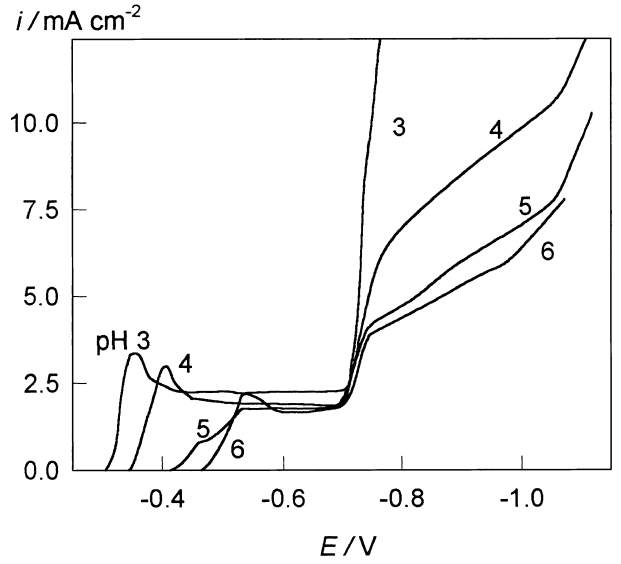

Fig. 3. Voltammograms of Sn and Co codeposition recorded at various pH indicated on the curves. Conditions of natural convection. Sn(II) 0.05 M; Co(II) 0.2 M; Cit 0.1 M.

for the complicated voltammogram shape [24, 26]. This may be illustrated by the data presented in Figure 1: voltammograms of Sn(II) electroreduction exhibit irregularities which manifest themselves as prewaves at $-0.65\ V < E < -0.5\ V$. A sharp and deep decrease in the surface concentration of EAC, occurring at a certain i, is the reason for such behaviour [22, 24]. The limiting current plateau is well defined at $E < -0.7$ V.

Voltammograms of Co(II) reduction are less complicated (Figure 2). With increase in Co(II) concentration, both the open-circuit potential and the limiting current increase. However, in contrast to Sn(II) reduction, the limiting current observed at $E < -0.85$ V is less pronounced owing to the evolution of H_2 starting at about -0.9 V (see curve for $c_{Co(II)} = 0$).

Systems containing both metals show no new effects which differ from those mentioned above (Figures 3 and 4). Two limiting currents attributable to the reduction of Sn(II) and Co(II) are observed (cf. Figures 1–4). A correlation between the shape of the voltammograms and the degree of complexation is seen from Figure 3 where the influence of pH is shown. There the shift in the Sn|Sn(II) equilibrium potential is clearly observed with increase in pH. The data further show that the polarization of H_2 evolution decreases with increasing solutions acidity. The hydrogen partial current masks

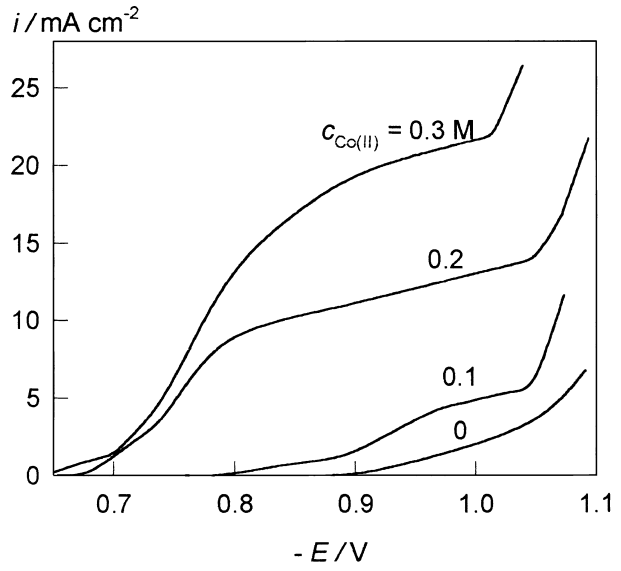

Fig. 2. Experimental voltammograms of Co(II) reduction recorded under natural convection conditions. Total concentration of Co(II) is indicated on the curves. Cit 0.3 M pH 4.

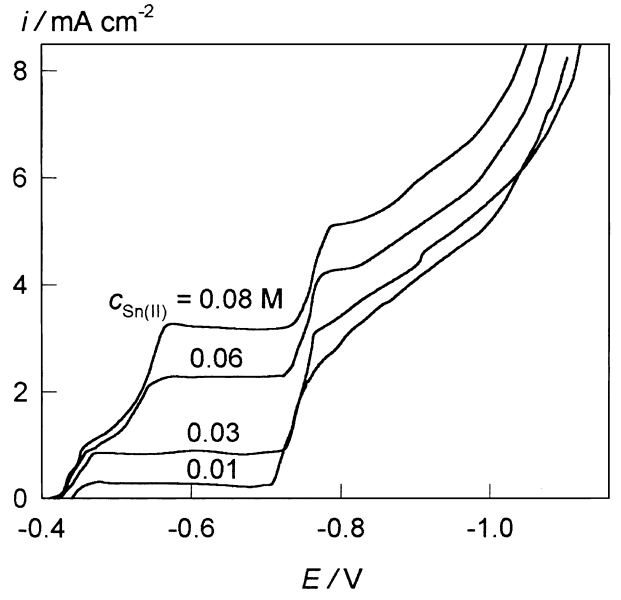

Fig. 4. Voltammograms of Sn and Co codeposition recorded under natural convection conditions. Co(II) 0.1 M; Cit 0.1 M; pH 5. Total concentration of Sn(II) is indicated on the curves.

completely the limiting current of Co(II) reduction at pH 3.

Figure 4 illustrates the influence of Sn(II) concentration on the overall process. The first limiting current increases with the Sn(II) concentration affecting the position of the voltammograms at $E < -0.65$ V where the second partial process of Co(II) reduction also occurs.

An example of partial voltammograms determined by the analysis of coatings (see experimental part) is presented in Figure 5. To determine the initial potential of Co(II) reduction, let us imagine that a small crystal of cobalt is inserted into a tin coating under open circuit conditions. The comparison of equilibrium potentials obtained with Nernst equations involving simulated $[Sn^{2+}]$ or $[Co^{2+}]$ yields that $E_{eq}^{Sn} > E_{eq}^{Co}$. Since the open-circuit potential $E_{oc} \approx E_{eq}^{Sn}$ (the surface area of tin is supposed to be much larger than that of cobalt), the Co crystal is polarized anodically and should be dissolved. A decrease in electrode potential E gives rise to Sn deposition and to release of a certain amount of ligand which, in turn, reacts with Co^{2+} ions decreasing their surface concentration. Similarly, E_{eq}^{Co} may be determined by the Nernst equation involving $[Co^{2+}]_s$ as a function of the current density i. According to the results of the simulation, the equality $E = E_{eq}^{Co} = -0.32$ V becomes valid at the certain i, which accounts for about 80% of the limiting current of Sn(II) reduction. Consequently, Co(II) reduction is possible at more negative potentials.

Co(II) reduction in the solution of given composition (Figure 5) starts at about -0.62 V. Similar results were obtained for solutions containing lower amounts of Co(II) (0.1 M). They show that Co(II) reduction on a foreign (Sn) substrate occurs with large overvoltage.

The experimental voltammograms recorded under natural convection conditions indicate some features which actually are not observed when the r.d.e. technique is applied. Such effects as the occurrence of the current maxima or variations of the limiting current with ligand concentration or pH seem to be caused by instabilities in the diffusion layer the thickness of which depends on the current density. Due to well-defined regularities of mass transport under forced convection conditions, the r.d.e. technique seems to be more preferable for kinetic studies.

Although the analysis of kinetics and mechanism does not constitute the main object of the present paper, it is appropriate to consider some problems relating, first and foremost, to the processes proceeding at pH 4, which were not reflected in [22]. An example of simulated variations in the surface concentration of the species in the cobalt-free solution is given in Figure 6. There the cathodic i is normalized to the limiting current density (i_d) of Sn(II) reduction. Attention should be drawn to the fact that the surface concentration of SnL^{2-} increases with i/i_d up to $i/i_d < 0.4$. Such an effect results from shifts in chemical equilibria at the electrode surface and is impossible for simple ligand-free systems. This phenomenon provides a convincing explanation for a abnormally high slope of the experimental voltammogram.

The simulated data in Figure 6 were used for constructing normalized Tafel plots (NTP) presented in Figure 7. Their linear approximation makes it possible to determine the kinetic parameters, i_0 and α, on the basis of Equation 3.

Slopes of the two given NTP (Figure 7) are slightly dependent on the solution composition, whereas i_0 values obtained by extrapolation of NTP to E_{eq}^{Sn} are much higher for cobalt-free solutions. This correlates with the changes in the bulk concentration of SnL^{2-} complexes.

Only a part of the experimental data obtained within the region of high overvoltages was used to construct

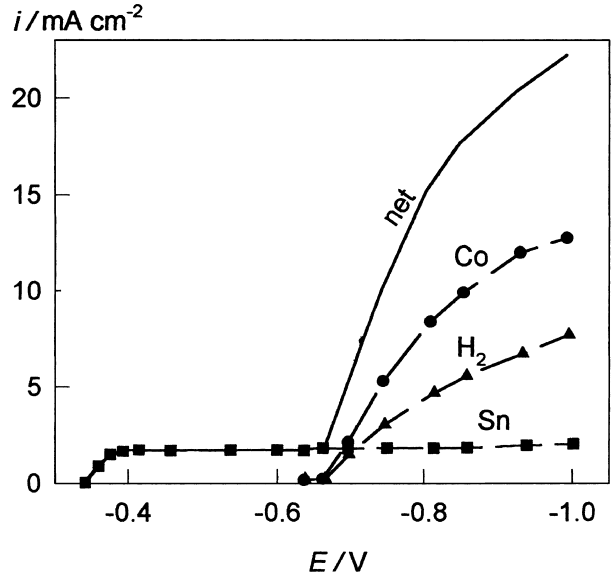

Fig. 5. Net (full line) and partial (symbols, dotted lines) voltammograms for the indicated solution compositions. Sn(II) 0.05 M; Co(II) 0.3 M; Cit 0.1 M; pH 4.

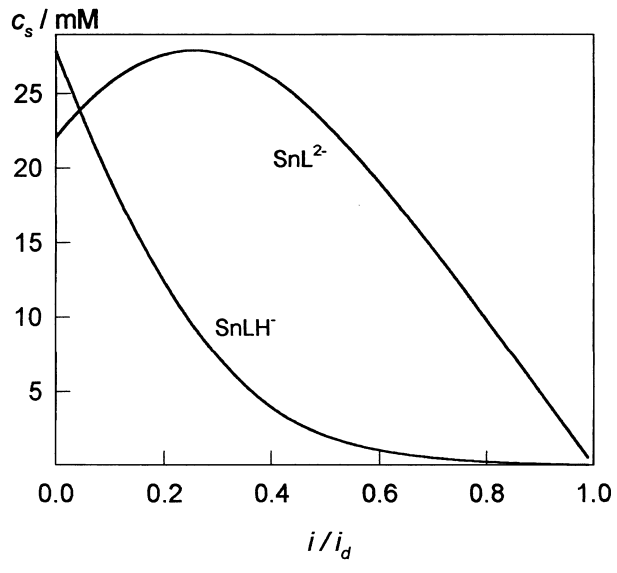

Fig. 6. Variations of surface concentrations of species indicated on the curves with the normalized cathodic current density. Sn(II) 0.05 M; Cit 0.75 M; pH 4.

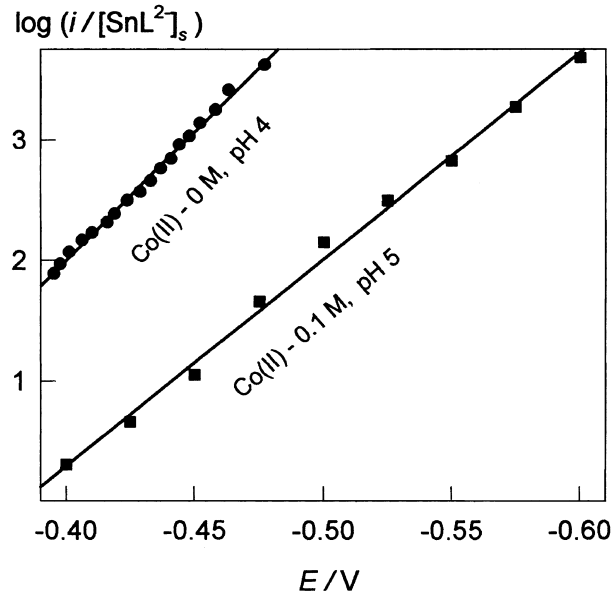

Fig. 7. Tafel plots normalized to the surface concentration of SnL^{2-} for various solution composition. Rotating velocity of r.d.e. is 450 rpm. Sn(II) 0.05 M; Cit 0.075 M.

NTP. Therefore, to check the correctness of the deduced kinetic parameters, the entire voltammogram was calculated by Equation 2. The simulated data (lines) are in good agreement with the experimental data (points) and properly represent a sharp rise of the voltammogram at $-0.5\ V < E < -0.4\ V$ for the process of $SnL^{2-} + 2\ e^- \rightarrow Sn + 2L^{4-}$ (Figure 8).

A similar procedure was used in analysing the partial process of Co(II) reduction (see the right curve in Figure 8). As has been mentioned above, this process starts at $E \approx -0.6$ V. Taking it into the consideration,

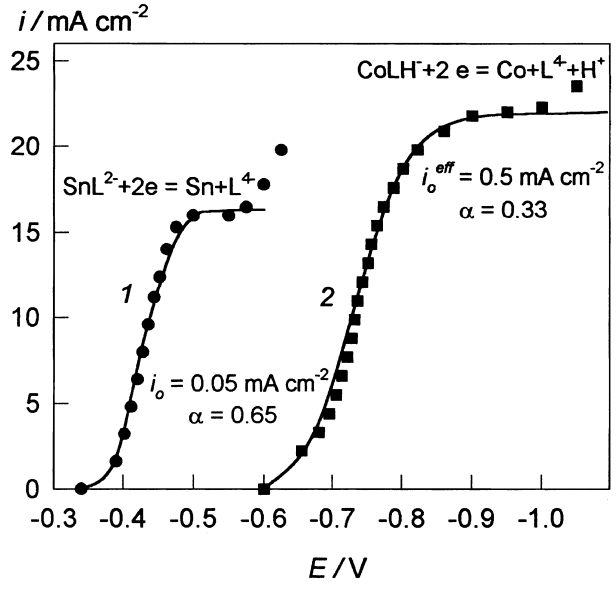

Fig. 8. Comparison of voltammograms simulated for the indicated partial processes (lines) and obtained experimentally (symbols) at 450 rpm. Solution compositions: Sn(II) 0.05 M, Cit 0.075 M, pH 4 (left curve) and Sn(II) 0.05 M, Co(II) 0.1 M, Cit 0.075 M , pH 5 (right curve).

the effective current density (i_0^{eff}) was defined at this potential.

5. Effect of solution composition and electrolysis conditions on the characteristics of Sn–Co coatings

As mentioned above, the degree of Sn(II) complexation should be much higher than that of Co(II) in the optimum case. Such condition can be reached in the system with ligand deficit in which Sn(II) is properly complexed and the most of the Co(II) is in the form of aqua-ions. This conclusion is substantiated by the elemental composition of Sn–Co coatings. For example, when ligand concentration is increased twofold (from 0.2 to 0.4 M) in the solution containing 0.05 M of Sn(II), 0.1 M of Co(II) at pH 5, the amount of Co decreases tenfold (from 35 to 3.4 mass %). Moreover, coatings formed in the latter case are uneven and incompact. That is why 0.1 M concentration citrate may be chosen as optimum. Although the difference in equilibrium potentials remains sufficiently large, zones of the limiting current for both metals come close to each other. It is important that the degree of Co(II) complexation should be low, because otherwise the evolution of hydrogen starts to dominate within the region of codeposition, resulting in the decrease in cobalt current efficiency.

In this respect, pH is also of importance. If pH is too low, the effects of complexation become weaker. For example, the amount of a more electronegative component (Co) in coatings was found to decrease at pH 3 due to significant depolarization of H_2 observed in the acid medium (see Figure 3). According to our evaluation, optimal pH varies from 4 to 5.9. Then the amount of cobalt is stable within a rather large range of current densities.

It follows from model simulations that the surface pH increases significantly with cathodic current density. This effect results from corresponding shifts in equilibria given above and occurs even when hydrogen evolution does not occur. Then $[Sn^{2+}]\ [OH^-]^2$ or $[Co^{2+}]\ [OH^-]^2$ products simulated for the electrode surface may exceed those determined by the solubility constant (K_{so}) of $Sn(OH)_2$ or $Co(OH)_2$, respectively. The simulated data that illustrate this statement are presented in Figure 9. They give sufficient grounds to draw the conclusion about the possibility of forming metal hydroxides at certain current densities and the bulk pH. Hydroxides may form colloidal species and act as brighteners. Oversaturation of the surface layer should not be too high. This may be achieved by using H_3BO_3 as a buffer which improves the structure of coatings.

The influence of Sn(II) concentration on the coating composition may be seen from the data presented in Figure 10. Content of Sn and Co vary almost linearly with $c_{Sn(II)}$. At the same time, the amount of oxygen included in the coatings increases with the content of Co. It may be concluded that the source of oxygen can be $Co(OH)_2$ formed at the electrode surface.

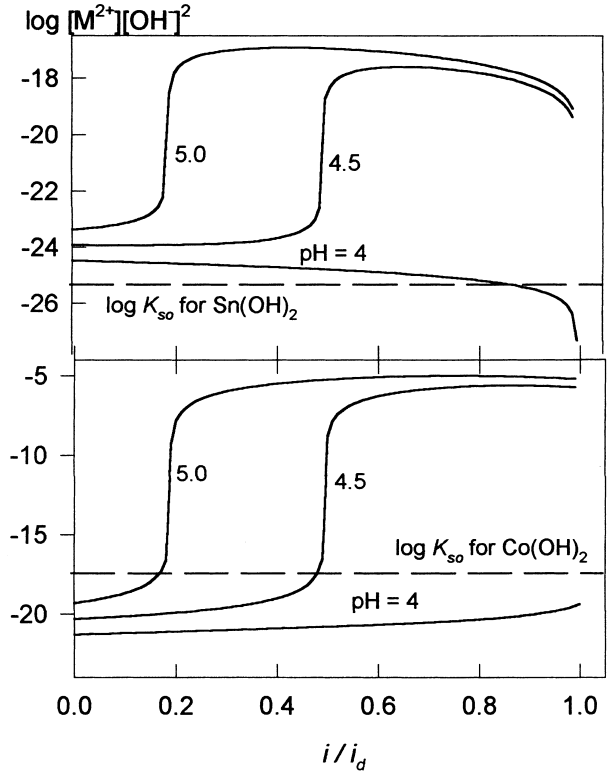

Fig. 9. Comparison of solubility products of $Sn(OH)_2$ and $Co(OH)_2$ (dotted lines) with the corresponding magnitudes (full lines) obtained from calculated surface concentrations of Sn^{2+}, Co^{2+} and OH^- at various bulk pH indicated on the curves. Sn(II) 0.05 M; Co(II) 0.1 M; Cit 0.1 M.

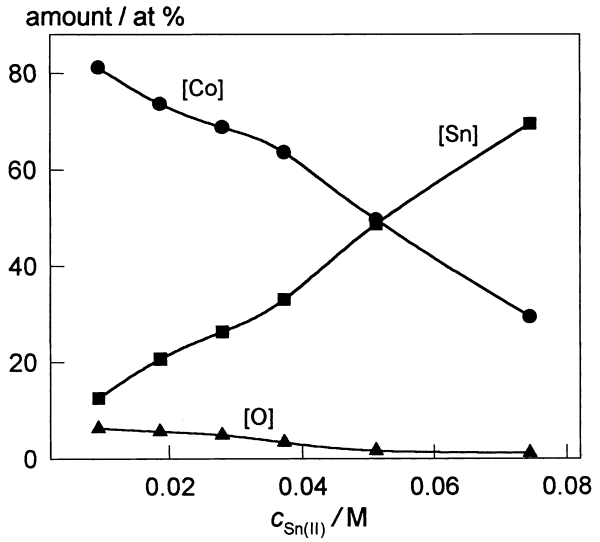

Fig. 10. Variations of elemental composition in the surface of coatings deposited at 10 mA cm^{-2} from solutions containing different total concentration of Sn(II). Co(II) 0.1 M; Cit 0.1 M; H_3BO_3 0.3 M; pH 4.5.

As has been mentioned above, codeposition of Sn and Co begins within the region of the limiting current of the first metal. Each metal forms separate phases at initial stages of alloy crystallization, unevenly located in the coating. They can be observed visually as separate white (Sn) and deep gray (Co) zones. Evidently, Co forms a separate phase due to a considerable overvoltage of Co crystallization on a foreign (Sn) substrate. With increase in the current density (when the potential becomes more negative), the amount of a deep gray (Co) phase increases as long as the compact coating containing about 80 mass % of Co is formed. This state corresponds to a fairly constant (about −0.9 V) potential although current densities can be different in solutions of different composition.

When cathodic polarization slightly increases and the alloy composition changes up to 76 mass % of Co, bright coatings are obtained. Quite a high rate of H_2 evolution (see Figure 5) can cause alkalinization of the surface layer sufficient for $Co(OH)_2$ to form. This is corroborated by the data obtained by X-ray photoelectron spectroscopy showing correlation between the amount of cobalt and oxygen in the surface of the coating (Figure 10). Oxygen binding energy was established to be equal to 531.2 eV; the same value is given for both $Co(OH)_2$ and CoOOH in [28]. Etching of the electrode surface by Ar^+ shows that the amount of oxygen decreases with the thickness of the coating and tends to zero at the depth of 40 nm. The source of oxygen might be Co(II) hydroxides capable of forming gel type aggregates [29] which, in turn, can cause the brightening effect.

Broad XRD peaks were observed within the scanned 2θ range. The maxima of the peaks correspond to the following d values: 0.2062, 0.1267 and 0.1079 nm which may be attributed to the β-Co phase, as well as to that of α-Co. Figure 11(a) represents a fragment of the XRD pattern of the Sn–Co coating containing 86 mass % of Co. This broad peak was analysed using the XRD peak separation program accounting for the gaussian intensity distribution. As a result of the analysis, three broad and one sharp peaks were obtained. The maxima of the first three peaks corresponded to the following d values: 0.2171, 0.2056 and 0.1964 nm. These peaks could be attributed to the α-Co phase with increased crystal lattice parameters caused by the replacement of some cobalt atoms by tin atoms having a larger atomic radii. The sharp peak is attributable to the β-Co phase with increased crystal lattice. Thus, the Sn–Co coating containing 86 mass % of Co could be considered to be solid solution of tin in α-Co and β-Co. Both latter phases were found to be formed only in solutions of Co(II) containing some brighteners [30]. In contrast to the data reported in [17, 20], no evidence is available in XRD patterns for intermetallic Sn–Co phases such as γ'-Co_3Sn_2 or $CoSn_2$.

The β-Sn phase is predominant in the coating containing 37 mass % of Co (Figure 11(b)). There are some additional peaks: that of the Cu substrate and another that cannot be attributed to any known phase involving Co or Sn.

Sn–Co coatings containing from 15 to 86 mass % of Co can be obtained in solutions under discussion. The

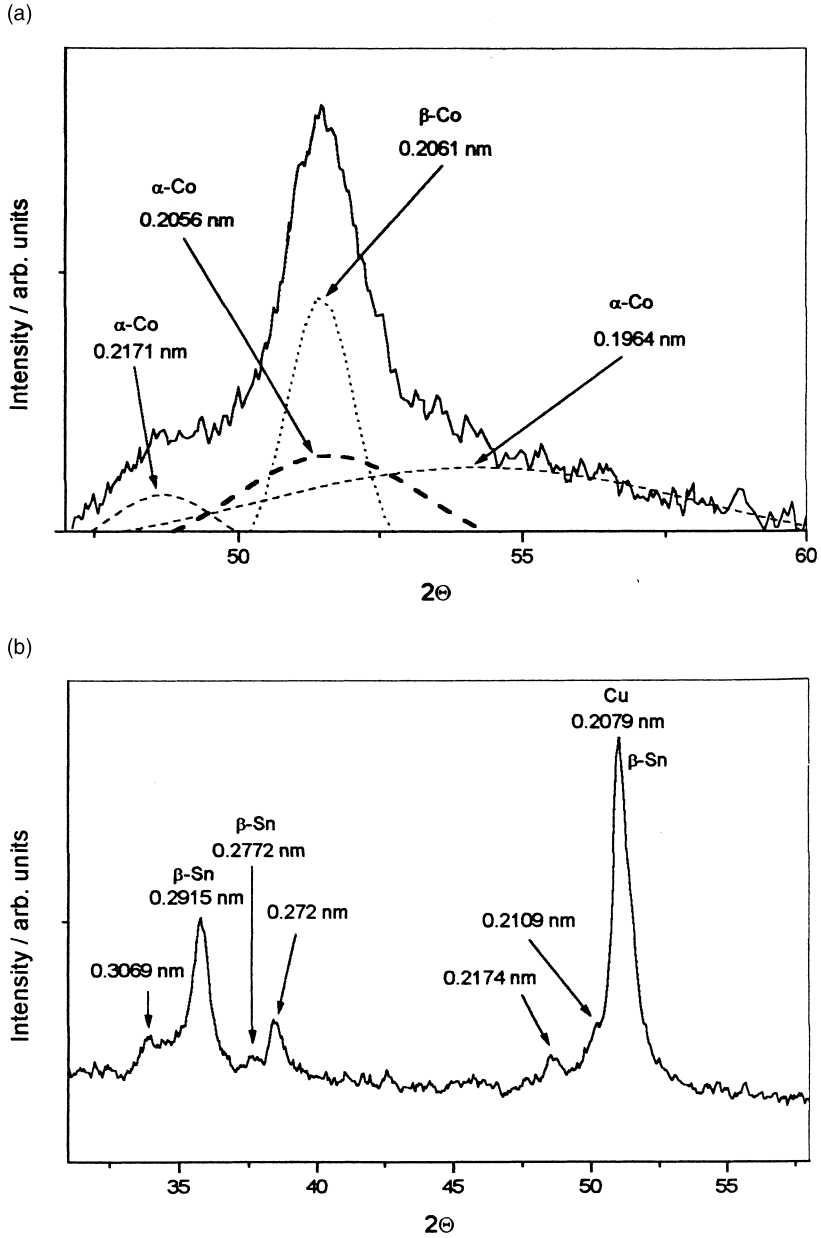

Fig. 11. X-ray diffraction patterns of Sn–Co coatings containing (a) 86 (the sample removed from the substrate) and (b) 37 mass % of Co. Line of Cu in (b) comes from the substrate.

coating composition may also be adjusted by means of various surface-active substances which exert a selective influence over the rate of partial processes.

6. Conclusions

The model involving equilibrium characteristics and mass transport of Sn(II) and Co(II) citrate complexes yields valuable information on the distribution of complex species in the bulk and at the electrode surface. It enables optimal solution compositions and electrolysis conditions to be selected for Sn and Co codeposition.

Optimal conditions for Sn and Co codeposition are achieved in slightly acid citrate solutions containing no excess of ligand. The partial voltammograms of Sn(II) and Co(II) reduction may be described quantitatively with the proviso that SnL^{2-} and $CoLH^{-}$ are electrically active complexes. Sn–Co coatings containing from 15 to 86 mass % of Co can be deposited.

Colloids of Sn(II) and Co(II) hydroxides formed at the electrode surface seem to act as brighteners. Bright deposits may be obtained when the Co content exceeds 76%. Then coatings could be considered to be solid solutions of tin in α-Co and β-Co. The β-Sn phase is predominant in coatings containing less Co.

References

1. A. Brenner, 'Electrodeposition of Alloys', Vol. 1 (Academic Press, New York, 1963).
2. B.F. Müller, *Jakob. Oberflächentech.* **32** (1976) 303.

3. A.S. Knodler, *Jakob. Oberflächentech.* **33** (1977) 166.
4. A.H. Chapman, W.B. Hampshire and D.J. Maykuth, *Plat. Surf. Finish.* **70** (1983) 40.
5. R. Ott, *Galvanotechnik* **49** (1995) 10.
6. A. Liebscher, *Galvanotechnik* **88** (1997) 754.
7. J. Cuthbertson, *J. Electrodep. Techn. Soc.* **27** (1951) 13.
8. H. Miyashita and S. Kurikawa, *J. Metal Finish. Soc. Japan* **21** (1970) 79.
9. M. Clark, R.C. Elbourne and C.A. Mackay, *Trans. Instit. Metal Finish.* **50** (1972) 180.
10. *US Patents 2 336 615* (1943), *2 658 866* (1953), *3 772 168* (1973), *3 881 919* (1975), *3 914 160* (1975), *3 966 564* (1976), *4 035 249* (1977), *4 428 803* (1984).
11. *Japanese Patents 55-12 111* (1980), *58-58438* (1983), *75-13313* (1986), *85-10997* (1988).
12. *UK Patent GB 2 094 349* (1982).
13. A.E. Davis, *Trans. Inst. Metal Finish.* **31** (1954) 401.
14. V. Sree and T.L. Rama-Char, *J. Electrochem. Soc. (India)* **9** (1960) 13.
15. Y. Tsuji and M. Ishikawa, *Corrosion* **27** (1971) 168.
16. J.D.C. Hemsley and M.E. Roper, *Trans. Inst. Metal Finish.* **57** (1979) 77.
17. J. Jaen, M.L. Varsanyi, E. Kovacs, I. Czako-Nagy, A. Buzas, A. Vertes and L. Kiss, *Electrochim. Acta* **29** (1984) 1119.
18. K. Tyutina, L. Lukyanova and G. Selivanova, *Zaschita Metallov* **30** (1984) 484.
19. P. Kopteva, K. Tyutina, L. Kosmadamyanskaya, A. Popov and G. Selivanova, *37th ISE Meeting. Extended Abstracts*, Vol. 2 (Vilnius, 1986), p. 281.
20. S.S. Abd El Rehim, S.A. Refaey, G. Schwitzgebel, F. Taha and M.B. Saleh, *J. Appl. Electrochem.* **26** (1996) 413.
21. G.I. Medvedev, V.I. Zhuravlev, N.Yu. Fursova and I.P. Gan'shina, *Zh. Prikl. Khim.* **71** (1998) 937.
22 A. Survila, Z. Mockus and S. Kanapeckaite, *Electrochim. Acta* **46** (2000) 565.
23. C.D. Wagner, W.M. Riggs, L.E. Davis, J.F. Moulder, G.E. Muilenberg, 'Handbook of X-ray Photoelectron Spectroscopy.' (Minnesota, Perkin–Elmer Corp., 1978).
24. A. Survila, 'Electrode Processes in Systems of Labile Complexes of Metals' (in Russian), (Mokslas, Vilnius, 1989).
25. R. Šarmaitis and A. Survila, *Plat. Surf. Finish.* **85** (1998) 64.
26. A. Survila and P.V. Stasiukaitis, *Electrochim. Acta* **42** (1997) 1113.
27. A. Survila and V. Uksienė, *Electrochim. Acta* **37** (1992) 745.
28. N.S. McIntyre and M.G. Cook, *Analyt. Chem.* **47** (1975) 2208.
29. V. Parfionov and V. Račinskas, *Lietuvos MA Darbai. B. Serija* **3** (118) (1980) 35.
30. I. Kirilova, I. Ivanov and S. Rashkov, *Bulg. Chem. Commun.* **29** (1997) 204.